Synthesis and Characterization of Thieno[3,2-b]thiophene-isoindigo-based Copolymers as Electron Donor and Hole Transport Materials for Bulk-Heterojunction Polymer Solar Cells

Xiaofeng Xu,[1] Ping Cai,[2] Yong Lu,[1] Ng Siu Choon,[1] Junwu Chen,[2] Xiao Hu,[3] Beng S. Ong[1,4]

[1]School of Chemical and Biomedical Engineering, Nanyang Technological University, Singapore 637459
[2]State Key Laboratory of Luminescent Materials and Devices, Institute of Polymer Optoelectronic Materials and Devices, South China University of Technology, Guangzhou 510640, China
[3]School of Materials Science and Engineering, Nanyang Technological University, Nanyang Avenue, Singapore 639798
[4]Institute of Creativity and Department of Chemistry, Hong Kong Baptist University, Hong Kong, China
Correspondence to: Ng. S. Choon (E-mail: NgSC@ntu.edu.sg) or B. S. Ong (E-mail: bong@hkbu.edu.hk)

Received 19 August 2012; accepted 30 September 2012; published online 19 October 2012
DOI: 10.1002/pola.26400

ABSTRACT: A novel class of thieno[3,2-b]thiophene (TT) and isoindigo based copolymers were synthesized and evaluated as electron donor and hole transport materials in bulk-heterojunction polymer solar cells (BHJ PSCs). These π-conjugated donor-acceptor polymers were derived from fused TT and isoindigo structures bridged by thiophene units. The band-gaps and the highest occupied molecular orbital (HOMO) levels of the polymers were tuned using different conjugating lengths of thiophene units on the main chains, providing band-gaps from 1.55 to 1.91 eV and HOMO levels from -5.34 to -5.71 eV, respectively. The corresponding lowest unoccupied molecular orbital (LUMO) levels were appropriately adjusted with the isoindigo units. Conventional BHJ PSCs (ITO/PEDOT:PSS/active layer/interlayer/Al) with an active layer composed of the polymer and $PC_{71}BM$ were fabricated for evaluation. Power conversion efficiency from a low of 1.25% to a high of 4.69% were achieved with the best performing device provided by the D$-\pi-$A polymer with a relatively board absorption spectrum, high absorption coefficient, and more uniform blend morphology. These results demonstrate the potential of this class of thieno[3,2-b]thiophene-isoindigo-based polymers as efficient electron donor and hole transport polymers for BHJ PSCs. © 2012 Wiley Periodicals, Inc. J Polym Sci Part A: Polym Chem 51: 424–434, 2013

KEYWORDS: bulk-heterojunction polymer solar cells; charge transport; conjugated polymers; isoindigo; optical properties; thieno[3,2-b]thiophene

INTRODUCTION During the past decade, polymer solar cells (PSCs) have attracted growing attention from academic and industry communities as a potentially viable solar energy harvesting medium by virtue of their ability in providing light weight and large-area devices at low manufacturing costs.[1,2] The low manufacturing cost is made possible via conventional low-cost solution-based fabrication techniques such as coating and printing. From this perspective, bulk-heterojunction polymer solar cells (BHJ PSCs), which utilize a solution-processed active layer composed of an electron donor/hole transport component and an electron acceptor/electron transport counterpart, sandwiched between an ITO anode and a low work-function metal cathode, have been intensively investigated.[3–6] For optimum cell performance, broad-absorption and narrow band-gap polymers would be highly desirable as they are more efficient in capturing solar energy.[7–12] In general, narrow band-gap polymers can be constructed from a polymer framework with an alternating electron-rich donor (D) and an electron-deficient acceptor (A) repeating unit, The conjugated D$-$A polymer system offers an opportunity for tuning the band-gaps and energy levels through the donor and acceptor strengths and nature of π-conjugation. An ideal electron donor/hole transport polymer for BHJ PSC would require a low-lying HOMO level to ensure a high open-circuit voltage (V_{oc}) and an intense broad absorption spectrum to maximize the short circuit current (J_{sc}). In addition, the polymer should enable formation of proper morphology with continuous nanostructures of hole and electron transport components with maximum interfacial areas as the morphology has a profound influence on exciton dissociation, and thus the performance of BHJ PSC.[13] Likewise, interfacial modification between the active layer and electrodes can also facilitate extraction of exciton into respective electrodes, which would lead to further improvements in photovoltaic performance.[14–16] To date, many structurally diverse systems of narrow band-gap polymers have been synthesized for use in BHJ PSCs, with the power conversion efficiency (PCE) reaching up to 8%.[17–27] Nevertheless, the rational design of novel D–A conjugated copolymers with good photovoltaic property remains a key interest in synthesis. Driving organic photovoltaic PCE up to an economically viable level would require further development in electron donor and hole transport materials.

Not surprisingly, we have recently witnessed intense activities in exploring new electron donor and acceptor structures for building more efficient hole transport polymers. In this respect, the isoindigo-based acceptors have been utilized with different electron-rich moieties (e.g., thiophene, bithiophene, terthiophene, and benzodithiophene) for the construction of D–A polymers.[28–33] One of these copolymers exhibited promising photovoltaic results in BHJ PSCs with PCE reaching as high as 6.3%,[34] In addition, this class of D–A polymers as stable active materials have also shown high hole mobility in organic field-effect transistors.[35] Nonetheless, several research about isoindigo-based D–A polymers exhibited limited PCE below 3%. One of the challenges besetting the isoindigo-based D–A polymers is poor solubility due to the rigid ketopyrrole cores. This difficulty in attaining either highly ordered molecular assembly or favorable layer morphology has adversely affected the device performance.

In this article, we report the synthesis of four novel thieno[3,2-b]thiophene (TT) and isoindigo based copolymers, **P1**, **P2**, **P3,** and **P4** via Pd-catalyzed Stille coupling polymerization. The use of fused TT unit affords a strong electron-rich moiety, which may also enhance hole transporting properties of the resulting polymers.[36,37] Introduction of alkyl pendant chains into TT unit would serve to further increase the polymer solubility. The relatively planar structures of 2,5-bis(3-alkylthiophen-2-yl)-TT and 3,6-alkyl-2,5-di(thiophen-2-yl)-TT moieties on the polymer chains would be expected to facilitate $\pi-\pi$ stacking to attain more ordered molecular assembly of conjugated main chains, which can also extend the coplanarity of polymer backbones and would be conducive to intermolecular charge-carrier hopping.[38–40] In addition, the TT units can modify the effective conjugation length of polymer chains, thus suppressing the HOMO levels of some high-mobility polythiophenes.[38,41] A low-lying HOMO level is a precondition for high V_{oc} achievement for BHJ solar cells. The alternating TT and isoindigo moiety bridged by diverse *n*-alkylthiophene units afforded four narrow band-gap copolymers with different conjugated length of backbones. Their thermal stability, UV–vis absorption and electrochemical properties were investigated to understand their structure-property relationships. Polymers **P1**, **P2,** and **P3** exhibited good solubility characteristics and could be used in fabrication of BHJ PSCs. Conventional BHJ PSCs (ITO/PEDOT:PSS/active layer/interlayer/Al) with $PC_{71}BM$ as the electron acceptor/electron transport material and the conjugated polymer as electron donor/hole transport material were fabricated. In addition, various processing solvents and additives were also investigated to further improve on the device performance. The observed PCE of devices based on polymers **P1**, **P2,** and **P3** were 1.25, 4.69, and 3.24%, respectively. The film morphology of all the blend layers and the hole mobility of polymer **P2** were also investigated. Comparison of polymer main chains based on thieno[3,2-b]thiophene and isoindigo bridged with diverse *n*-alkylthiophene units will provide some useful information on the influence of D–π–A structure for photovoltaic properties of isoindigo-based copolymers.

EXPERIMENTAL

Materials

All reagents and solvents, unless otherwise specified, were obtained from Aldrich, Alfa Aesar, and TCI Chemical and were used as received. Anhydrous diethyl ether, tetrahydrofuran (THF) and toluene were distilled over sodium/benzophenone under N_2 prior to use. All manipulations involving air-sensitive reagents were performed under an argon atmosphere.

3,6-Dioctylthieno[3,2-b]thiophene,[37] 2,5-bis(trimethylstannyl) thieno[3,2-b]thiophene (5),[42] (*E*)-6,6′-dibromo-1,1′-bis(2- butyloctyl)-[3,3′-biindolinylidene]-2,2′-dione (6),[34] and (*E*)-6,6′-dibromo-1,1′-bis(2-octyldodecyl)-[3,3′-biindolinylidene]-2,2′- dione (7)[34] were prepared according to the literatures.

Measurements

^1H and ^{13}C NMR spectra were recorded on a Bruker AV 300 spectrometer with tetramethylsilane as the internal reference. Molecular weights of the polymers were obtained on a Waters 2695 GPC using a calibration curve of polystyrene standards, with THF as the eluent. Elemental analyses were performed on a Vario EL elemental analysis instrument (Elementar). UV–vis absorption spectra were recorded on a Shimadzu UV 2450 spectrophotometer. Thermogravimetric analysis (TGA) was carried out on a Perkin Elmer Diamond TGA/DTA, at a heating rate of 10 °C min^{-1} from 50 to 650 °C under a nitrogen atmosphere. Cyclic voltammetry was carried out on a CHI660A electrochemical workstation with platinum electrodes at a scan rate of 50 mV sec^{-1} against the Ag/Ag^+ reference electrode with an argon saturated solution of 0.1 M tetrabutylammonium hexafluorophosphate (Bu_4NPF_6) in acetonitrile (CH_3CN). The deposition of a polymer on the electrode was done by the evaporation of its dilute chlorobenzene (CB) solution.

Monomer Synthesis

2,5-Bis(trimethylstannyl)-3,6-dioctylthieno[3,2-b]thiophene (1)

To a mixture of 3,6-dioctylthieno[3,2-b]thiophene (0.55 g, 1.50 mmol) and *N,N,N,′N′*-tetramethylethylenediamine (TMEDA) (0.35 g, 3.0 mmol) in 20 mL of anhydrous diethyl ether was added a 1.6 M solution of *n*-BuLi in hexane (2.81 mL, 4.50 mmol) at 0 °C under an argon atmosphere. The reaction mixture was warmed to ambient temperature and stirred for 3 h. Then the reaction mixture was cooled to 0 °C again and Me_3SnCl (1.20 g, 6.00 mmol) was added in one portion. The reaction mixture was stirred at 0 °C for 30 min and then warmed to room temperature and stirred overnight. The resulting mixture was poured into water. The organic layer was extracted with hexane (50 mL), washed successively with water, and then dried over anhydrous $MgSO_4$. The solution was concentrated to afford the final compound as a light yellow liquid (0.99 g, 96%). ^{1}H NMR (300 MHz, $CDCl_3$), δ (ppm): 2.68 (t, $J = 7.9$ Hz, 4H), 1.55 (m, 4H), 1.28 (m, 20H), 0.89 (m, 6H), and 1.40 (s, 18H). ^{13}C NMR (75 MHz, $CDCl_3$), δ (ppm): 146.8, 141.8, 134.5, 32.4, 31.9, 30.1, 29.9, 29.5, 29.2, 22.7, 14.1, and -7.9. Anal. Calcd (%) for $C_{28}H_{52}S_2Sn_2$: C, 48.72; H, 7.59; S, 9.26. Found: C, 48.61; H, 7.75; S, 9.31.

3,6-Dioctyl-2,5-di(thiophen-2-yl)thieno[3,2-b]thiophene (3)

2,5-Dibromo-3,6-dioctylthieno[3,2-b]thiophene (1.34 g, 2.56 mmol), 2-(tributylstannyl)thiophene (2.39 g, 6.40 mmol), $Pd(PPh_3)_4$ (0.09 g, 0.08 mmol) were dissolved in 50 mL anhydrous THF. The reaction mixture was heated to 80 °C for 12 h under an argon atmosphere. After cooling to room temperature, the organic layer was extracted with dichloromethane (100 mL), washed successively with water and then dried over anhydrous $MgSO_4$. The residue was purified by column chromatography with hexane as the eluent to give the final compound as a yellow solid (1.12 g, 83%). ^{1}H NMR (300 MHz, $CDCl_3$), δ (ppm): 7.35 (d, $J = 7.8$ Hz, 2H), 7.17 (d, $J = 4.8$ Hz, 2H), 7.09 (m, 2H), 2.88 (t, $J = 7.9$ Hz, 4H), 1.75 (m, 4H), 1.28 (m, 20H), 0.89 (t, $J = 7.5$ Hz 6H). ^{13}C NMR (75 MHz, $CDCl_3$), δ (ppm): 138.5, 136.6, 132.0, 131.3, 127.5, 126.2, 125.7, 31.9, 29.7, 29.4, 29.2, 29.1, 28.8, 22.7, and 14.1. Anal. Calcd (%) for $C_{30}H_{40}S_4$: C, 68.13; H, 7.62; S, 24.25. Found: C, 68.25; H, 7.75; S, 24.28.

2,5-Bis(5-trimethylstannyl-thienyl-2yl)-3,6-dioctylthieno[3,2-b]thiophene (4)

To a mixture of 3,6-dioctyl-2,5-di(thiophen-2-yl)thieno[3,2-b]thiophene (**3**) (0.40 g, 0.76 mmol) and TMEDA (0.18 g, 1.52 mmol) in 15 mL of anhydrous diethyl ether was added a 1.6 M solution of *n*-BuLi in hexane (1.43 mL, 2.28 mmol) at 0 °C under an argon atmosphere. The reaction mixture was warmed to ambient temperature and stirred for 2 h. Then the reaction mixture was cooled to 0 °C again and Me_3SnCl (0.61 g, 3.04 mmol) was added in one portion. The reaction mixture was stirred at 0 °C for 30 min and then warmed to room temperature and stirred overnight. The resulting mixture was poured into water. The organic layer was extracted with diethyl ether (50 mL), washed successively with water, and then dried over anhydrous $MgSO_4$. The solution was concentrated to afford the final compound as a yellow liquid (0.60 g, 93%). ^{1}H NMR (300 MHz, $CDCl_3$), δ (ppm): 7.26 (m, 2H), 7.16 (d, $J = 3.6$ Hz, 2H), 2.88 (t, $J = 7.9$ Hz, 4H), 1.75 (m, 4H), 1.28 (m, 20H), 0.89 (m, 6H), 1.40 (s, 18H). ^{13}C NMR (75 MHz, $CDCl_3$), δ (ppm): 142.4, 138.6, 138.5, 135.5, 131.6, 131.5, 127.1, 31.9, 29.7, 29.3, 29.2, 29.0, 28.8, 22.7, 14.2, and -8.2. Anal. Calcd (%) for $C_{36}H_{56}S_4Sn_2$: C, 50.60; H, 6.61; S, 15.01. Found: C, 50.71; H, 6.78; S, 15.09.

(E)-1,1′-bis(2-octyldodecyl)-6,6′-bis(4-decylthiophen-2-yl)-[3,3′-biindolinylidene]-2,2′-dione (8)

(E)-6,6′-dibromo-1,1′-bis(2-octyldodecyl)-[3,3′-biindolinylidene]-2,2′-dione (**7**) (12.17 g, 12.40 mmol), 3-decyl-5-tributylstannylthiophene (15.92 g, 31.00 mmol), $Pd_2(dba)_3$ (0.03 g, 0.03 mmol), and $P(o\text{-}tol)_3$ (0.04 mg, 0.12 mmol) were dissolved in 80 mL anhydrous THF. The reaction mixture was heated to 80 °C for 12 h under an argon atmosphere. After cooling to room temperature, the organic layer was extracted with dichloromethane (100 mL), washed successively with water and then dried over anhydrous $MgSO_4$. The residue was purified by column chromatography with 1:10 (v/v) dichloromethane/hexane as the eluent to give the final compound as a purple solid (11.48 g, 73%). ^{1}H NMR (300 MHz, $CDCl_3$), δ (ppm): 9.15 (d, $J = 8.4$ Hz, 2H), 7.25 (m, 4H), 6.94 (d, $J = 1.2$ Hz, 4H), 3.68 (d, $J = 6.9$ Hz, 4H), 2.63 (t, $J = 7.7$ Hz, 4H), 1.91 (s, 2H), 1.65 (m, 4H), 1.28 (m, 92H), 0.88 (m, 18H). ^{13}C NMR (75 MHz, $CDCl_3$), δ (ppm): 168.6, 145.6, 144.7, 143.7, 137.9, 131.9, 130.1, 125.5, 120.9, 120.8, 119.0, 104.8, 44.4, 36.4, 31.93, 31.91, 31.8, 30.7, 30.5, 30.0, 29.9, 29.69, 29.67, 29.63, 29.60, 29.5, 29.4, 29.39, 29.37, 29.33, 28.3, 26.8, 26.7, 22.71, 22.69, 17.3, 14.1, and 13.6. Anal. Calcd (%) for $C_{84}H_{134}N_2O_2S_2$: C, 79.56; H, 10.65; N, 2.21; S, 5.06. Found: C, 79.67; H, 10.78; N, 2.29; S, 5.12.

(E)-6,6′-bis(5-bromo-4-decylthiophen-2-yl)-1,1′-bis(2-octyldodecyl)-[3,3′-biindolinylidene]-2,2′-dione (9)

N-Bromosuccinimide (NBS) (0.89 g, 5.02 mmol) in 10 mL *N,N*-dimethylformamide (DMF) was added dropwise into compound (**8**) (3.17 g, 2.5 mmol) in 50 mL chloroform over 30 min under an argon atmosphere. The reaction mixture was stirred at room temperature for another 30 min. The resulting mixture was poured into water. The organic layer was extracted with dichloromethane (100 mL), washed successively with water, and then dried over anhydrous $MgSO_4$. The residue was purified by column chromatography with 1:9 (v/v) dichloromethane/hexane as the eluent to give the final compound as a dark purple solid (3.30 g, 92%). ^{1}H NMR (300 MHz, $CDCl_3$), δ (ppm): 9.15 (d, $J = 8.4$ Hz, 2H), 7.18 (d, $J = 6.6$ Hz, 2H), 7.08 (s, 2H), 6.84 (s, $J = 1.5$ Hz, 2H), 3.67 (d, $J = 7.2$ Hz, 4H), 2.68 (t, $J = 7.7$ Hz, 4H), 1.90 (s, broad, 2H), 1.62 (m, 4H), 1.26 (m, 92H), 0.85 (m, 18H). ^{13}C NMR (75 MHz, $CDCl_3$), δ (ppm): 168.5, 145.7, 143.6, 143.3, 137.0, 131.8, 130.3, 124.9, 121.2, 118.5, 110.0, 104.4, 44.4, 36.4, 31.94, 31.93, 31.90, 31.8, 30.0, 29.8, 29.75, 29.70, 29.66, 29.64, 29.5, 29.4, 29.36, 29.35, 26.7, 22.7, and 14.1. Anal. Calcd (%) for $C_{84}H_{132}Br_2N_2O_2S_2$: C, 70.76; H, 9.33; N, 1.96; S, 4.50. Found: C, 70.85; H, 9.51; N, 2.05; S, 4.59.

General Procedure for Polymerization

The four polymers were synthesized by the same procedure of the palladium(0)-catalyzed Stille coupling reactions with a dibromide monomer and a bis(trimethylstannyl)-substituted monomer under an argon atmosphere.

Dibromide monomer 0.25 mmol of bis(trimethylstannyl)-substituted monomer, tris(dibenzylideneacetone)dipalladium(0) ($Pd_2(dba)_3$) (7 mg) and tri(*o*-tolyl)phosphine ($P(o\text{-}Tol)_3$) (9 mg) were dissolved in 15 mL of anhydrous toluene. The mixture was refluxed with vigorous stirring for 24 h under an argon atmosphere. After the mixture was cooled to room temperature, it was poured into 250 mL of methanol. The precipitated material was redissolved and filtrated through a funnel and precipitated again. The polymer was washed in a

Soxhlet extractor with acetone and hexane, and then Soxhlet-extracted with hot chloroform. The chloroform fraction was concentrated and poured into 250 mL of methanol. Finally, the precipitate was collected and dried in vacuum to afford the title polymer as a dark fiber.

Polymer P1. 260 mg. Yield: 72%. GPC: $M_n = 28.5$ kDa; $M_w/M_n = 2.3$. ^{1}H NMR ($CDCl_3$, 300 MHz), δ (ppm): 9.22 (br, 2H), 7.20–6.65 (m, 4H), 3.73 (br, 4H), 2.75 (br, 4H), 2.42 (br, 2H), 1.80–1.55 (m, 4H), 1.30–1.26 (m, 52H), 0.88 (br, 18H). Anal. Calcd (%) for $(C_{62}H_{90}N_2O_2S_2)_n$: C, 77.54; H, 9.38; N, 2.92; S, 6.67. Found: C, 77.22; H, 10.23; N, 2.10, S, 7.33.

Polymer P2. 359 mg. Yield: 76%. GPC: $M_n = 23.5$ kDa; $M_w/M_n = 1.9$. ^{1}H NMR ($CDCl_3$, 300 MHz), δ (ppm): 9.02 (br, 2H), 7.24–6.91 (m, 6H), 6.60 (br, 2H), 3.68 (br, 4H), 2.80 (br, 4H), 2.61 (br, 2H), 1.69 (br, 4H), 1.30–1.26 (m, 92H), 0.84 (br, 18H). Anal. Calcd (%) for $(C_{90}H_{134}N_2O_2S_4)_n$: C, 76.91; H, 9.54; N, 1.99; S, 9.11. Found: C, 75.71; H, 10.15; N, 2.24; S, 9.54.

Polymer P3. 388 mg. Yield: 68%. GPC: $M_n = 21.8$ kDa; $M_w/M_n = 2.1$. ^{1}H NMR ($CDCl_3$, 300 MHz), δ (ppm): 9.14 (br, 2H), 7.19–6.85 (m, 10H), 3.70 (br, 4H), 2.70 (m, 8H), 2.58 (br, 2H), 1.74–1.24 (m, 120H), 0.87 (br, 24H). Anal. Calcd (%) for $(C_{114}H_{170}N_2O_2S_6)_n$: C, 76.30; H, 9.48; N, 1.56; S, 10.71. Found: C, 74.98; H, 10.45; N, 1.91; S, 10.45.

Polymer P4. 234 mg. Yield: 51%. Anal. Calcd (%) for $(C_{86}H_{126}N_2O_2S_4)_n$: C, 76.55; H, 9.35; N, 2.08; S, 9.49. Found: C, 75.76; H, 10.15; N, 2.30; S, 9.25.

PSC Fabrication and Characterization

Patterned indium tin oxide (ITO) coated glass with a sheet resistance of 15–20 ohm/square was cleaned by a surfactant scrub and then underwent a wet-cleaning process inside an ultrasonic bath, beginning with deionized water followed by acetone and isopropanol. After oxygen plasma cleaning for 5 min, a 40 nm thick poly(3,4-ethylenedioxythiophene):poly(styrenesulfonate) (PEDOT:PSS) (Bayer Baytron 4083) anode buffer layer was spin-cast onto the ITO substrate and then dried by baking in a vacuum oven at 80 °C for overnight. The active layer, with a thickness in the range of 80–90 nm, was then deposited on top of the PEDOT:PSS layer by spin-coating from a CB or dichlorobenzene (DCB) solution. The interlayer solution in methanol was spin-coated on the top of the active layer to form a thin interlayer of 3–5 nm. The thickness of the PEDOT:PSS and active layer was verified by a surface profilometer (Tencor, Alpha-500). Determination of the thickness of the interlayer followed a previously published article.[43] At last, a 100 nm aluminum layer was thermally evaporated with a shadow mask at a base pressure of 3×10^{-4} Pa. The overlapping area between the cathode and anode defined a pixel size of 0.15 cm^2. The thickness of the evaporated cathodes was monitored by a quartz crystal thickness/ratio monitor (model: STM-100/MF, Sycon). Except the deposition of the PEDOT:PSS layers, all the fabrication processes were carried out inside a controlled atmosphere of nitrogen drybox (Vacuum Atmosphere) containing <10 ppm oxygen and moisture. The power conversion efficiencies of the resulting PSCs were measured under 1 sun, AM 1.5 G (air mass 1.5 global) spectrum from a solar simulator (Oriel model 91192). The current density−voltage ($J-V$) characteristics were recorded with a Keithley 2410 source unit. The external quantum efficiencies of PSCs were measured with a commercial photomodulation spectroscopic setup (DSR 100UV-B) including a xenon lamp, an optical chopper, a monochromator, and a lock-in amplifier operated by a PC computer (Zolix Instruments), and a calibrated Si photodiode was used as a standard.

RESULTS AND DISCUSSION

Synthesis of Monomers and Polymers

The synthetic routes for monomers are shown in Scheme 1. In the presence of excess *n*-BuLi and $(CH_3)_3SnCl$, 3,6-dioctylthieno[3,2-b]thiophene can be transformed to a bis(trimethylstannyl)-substituted monomer **1** in a 96% yield. TMEDA was used as a ligand, which can convert *n*-BuLi into a cluster with the higher reactivity during lithiation of 3-alkylthiophene. The 2,5-dibromo compound **2** was synthesized by bromination of compound **1** with NBS, with a yield of 89%. Compound **3** with a total yield of 83% was synthesized by Stille coupling of compound **2** and 2-(tributylstannyl)thiophene with $Pd(PPh_3)_4$ as the catalyst. A similar lithiation reaction of compound **3** afforded the target bis(trimethylstannyl)-substituted monomer **4** in a high yield of 93%. The isoindigo derivative **8** was synthesized by Stille coupling of compound **7** and 3-decyl-5-tributylstannylthiophene using $Pd_2(dba)_3$ and P(*o*-tol)$_3$ as the catalyst, with a yield of 73%. The 2,5-dibromo monomer **9** was synthesized by bromination of compound **8** with 2.01 equivalent of NBS in a 92% yield. The chemical structures of compounds **1**−**9** were confirmed using ^{1}H NMR, ^{13}C NMR and elemental analysis.

Scheme 2 shows the polymerization routes for the four target polymers. The preparations of the polymers **P1**, **P2**, **P3,** and **P4** were accomplished via $Pd_2(dba)_3$-catalyzed Stille reaction of the corresponding monomers. After polymerization, the crude polymers were purified by extracting with acetone, hexane, and chloroform in the Soxhlet extractor for hours. The chemical structures of **P1**, **P2,** and **P3** were confirmed by ^{1}H NMR and elemental analysis. Polymers **P1**, **P2,** and **P3** exhibited good solubility in many organic solvents, such as THF, chloroform, toluene, CB, and DCB. Polymer **P2** depicted better solubility in CB and DCB than **P1** and **P3**. However, after polymerization and precipitation in methanol, the crude polymer **P4** was found insoluble in most organic solvents like THF, chloroform and toluene. This polymer was only partially soluble in warm CB. In addition, since the 2,5-bis(3-decylthiophen-2-yl)-TT moiety affords better solubility than 3,6-octyl-2,5-di(thiophen-2-yl)-TT moiety, the polymer **P2** exhibited improved solubility in CB and DCB, in comparison to **P3** and **P4**. ^{1}H NMR measurement of polymer **P4** in $CDCl_3$ only showed weak and broad signals, indicating the polymer chains formed aggregates in the solution. We failed to obtain a thick and smooth film from the **P4** solution, thus hampering investigation of its absorption spectrum,

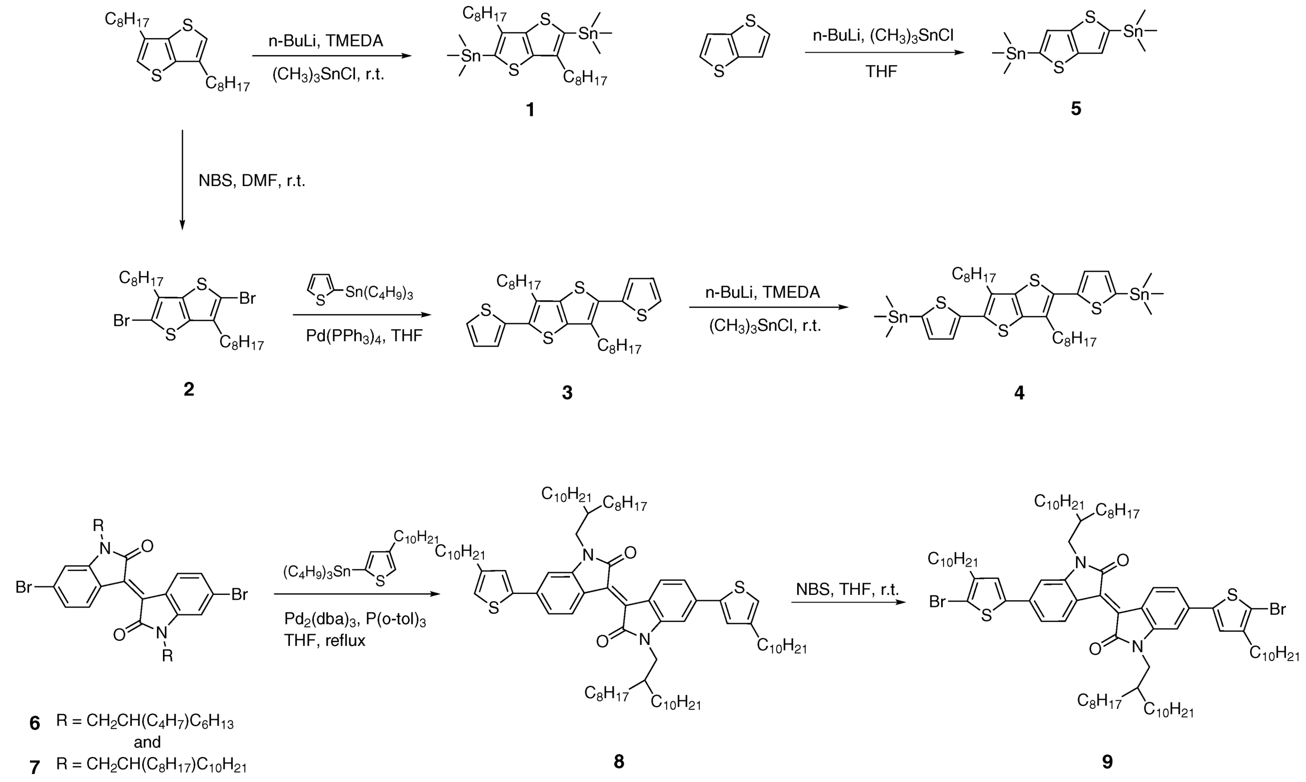

SCHEME 1 Monomer Synthesis.

electrochemical property and final device fabrication. The molecular weights of **P1**, **P2,** and **P3** as measured by GPC with calibration using polystyrene standards and THF as the eluent are listed in Table 1. The number-averaged molecular weights (M_n) of **P1**, **P2,** and **P3** are 28,500, 23,500, and 21,800 g mol^{-1} with polydispersity index (M_w/M_n) of 2.3, 1.9, and 2.1, respectively.

Thermal Stability

Thermal stability of the polymers was investigated using TGA, as shown in Figure 1. The TGA analysis shows the onset temperatures with 5% weight loss (T_d) of **P1**, **P2**, **P3,** and **P4** between 320 and 390 °C. These polymers are thus of sufficient stability for applications in optoelectronic devices.

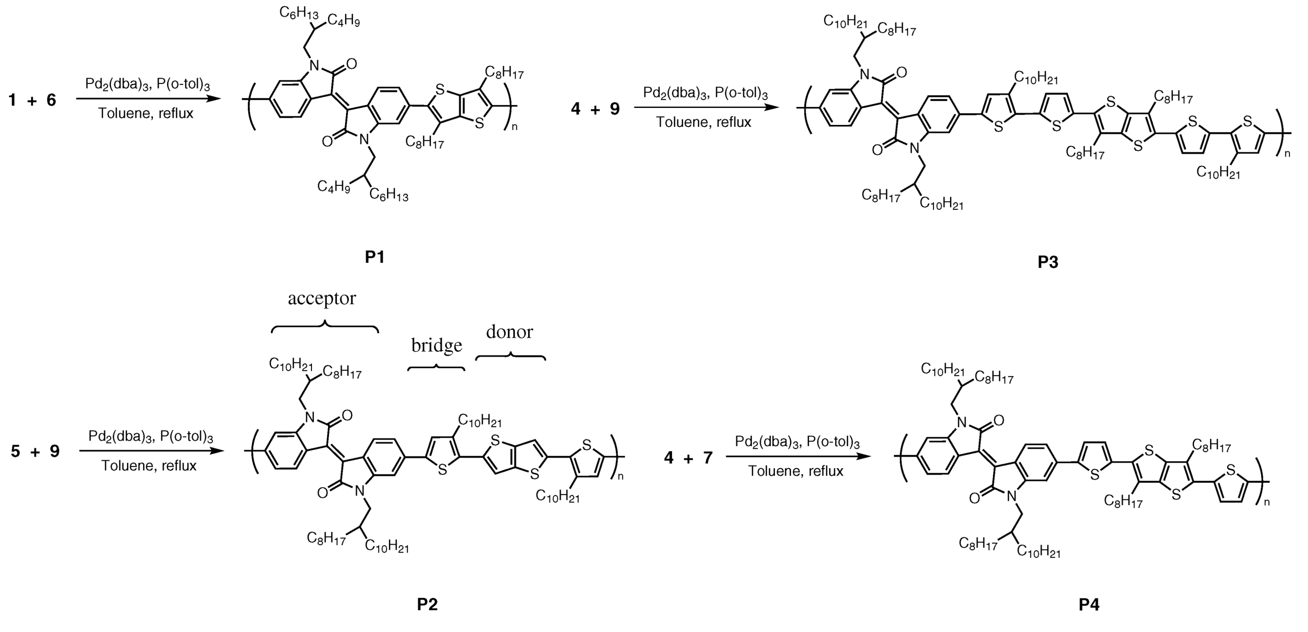

SCHEME 2 Polymer Synthesis.

TABLE 1 Molecular Weights and Thermal Properties of Polymers

Polymers	M_n[a]	M_w[a]	PDI[a]	T_d[b]
P1	28.5K	65.5K	2.3	389
P2	23.5K	44.6K	1.9	325
P3	21.8K	45.7K	2.1	359
P4	–[c]	–[c]	–[c]	374

[a] M_n, M_w, and PDI of the polymers were determined by GPC using polystyrene standards with THF as the eluent.

[b] The 5% weight loss temperatures under an inert atmosphere.

[c] No molecule weight received from GPC because of its limited solubility in THF.

Absorption Spectra

The UV–vis absorption spectra of polymers **P1**, **P2,** and **P3** in chloroform solutions and in film states are shown in Figure 2. The solution of **P1** shows one absorption band in the 400–750 nm range with absorption maximum (λ_{max}) at 610 nm (Table 2). When using alkylthiophene and alkylbithiophene as π-bridges between the TT and isoindigo units such as **P2** and **P3**, two distinct absorption bands in the wavelength ranges of 350–500 and 500–800 nm appear. This would be attributable to stronger D—A interaction and intramolecular charge transfer. The absorption maxima of **P2** and **P3** in chloroform are 630 and 625 nm, respectively. In comparison to **P2**, polymer **P3** containing *n*-alkylbithiophene π-bridges exhibit similar absorption spectrum in the 600–800 nm regions. However, **P3** has an obviously stronger absorption between 400 and 500 nm, which may be ascribable to the bithiophene moiety improving conjugation in the segment. In films, the λ_{max} value of **P1** is nearly the same with that in its solution, which exhibits a weak aggregation effect in the absorption spectrum. Its absorption edge for the absorption spectra of the film is at 765 nm. The λ_{max} value for the solid films of **P2** and **P3** are red-shifted to 644 and 647 nm, respectively, which is typically ascribable to the improved stacking and aggregation of the conjugated main chains in film phases. In comparison to the absorption curves in solutions, **P2** and **P3** films exhibit a distinct absorption shoulder from 700 to 750 nm, respectively, which is indicative of stronger interchain interactions of conjugated backbones in the condensed phase. The absorption edge of **P2** and **P3** are at 830 and 817 nm in solid films, respectively. The absorption coefficient of a solid film is also an important parameter for a narrow band gap polymer. A relatively large absorption coefficient means the incident beam is quickly attenuated on passage through a polymer film, which translates to more light being absorbed. The polymers **P1** and **P3** exhibit similar absorption coefficients of 0.35×10^{-2} nm^{-1} and 0.36×10^{-2} nm^{-1}, respectively. The absorption coefficient of polymer **P2** is higher than those of **P1** and **P3**, which is up to 0.61×10^{-2} nm^{-1}. The larger absorption coefficient may be attributable to its more favorable π—π stacking of polymer main chain in solid state.

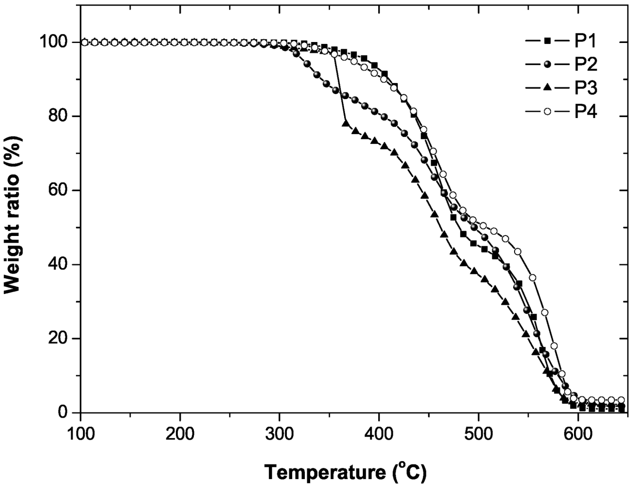

FIGURE 1 TGA plots of the polymers with a heating rate of 10 °C min^{-1} under an inert atmosphere.

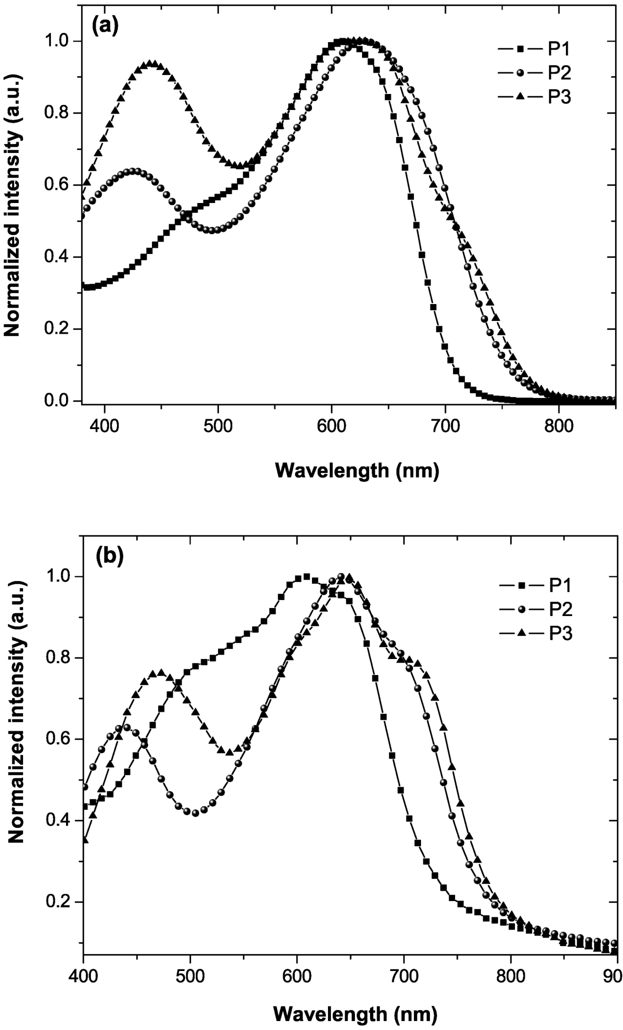

FIGURE 2 Normalized UV–vis absorption spectra of polymers: (a) in chloroform solutions; (b) in solid films.

Energy Level

Cyclic voltammetry (CV) measurements were performed for determining the highest occupied molecular orbital (HOMO)

TABLE 2 Optical and Electrochemical Properties of Polymers

	UV–vis absorption spectra				Cyclic voltammetry		
	Solution	Film			p-Doping	n-Doping	
polymer	λ_{abs}[a] (nm)	λ_{abs}[b] (nm)	λ_{onset} (nm)	E_g^{opt} (eV)[c]	φ_{ox}/HOMO (V)[d]/(eV)[e]	φ_{red}/LUMO (V)/(eV)[f]	E_g^{ec} (eV)[g]
P1	610	609	765	1.62	1.16/−5.71	−0.75/−3.80	1.91
P2	630	644	830	1.49	0.79/−5.34	−0.76/−3.79	1.55
P3	625	647	817	1.52	0.88/−5.43	−0.74/−3.81	1.62

[a] Absorption peak in chloroform solution.
[b] Absorption peak in film.
[c] Optical band gap.
[d] Onset voltage of oxidation process during cyclic voltammetry with Ag/Ag$^+$ reference electrode.
[e] Calculated according to HOMO $= -e(E_{ox} + 4.55)$ (eV).
[f] LUMO $= -e(E_{red} + 4.55)$ (eV).
[g] Electrochemical band gap.

and the lowest unoccupied molecular orbital (LUMO) energy levels and the electrochemical band gaps of the conjugated polymers. Figure 3 shows the cyclic voltammograms of the polymer films on Pt disk electrode in a 0.1M Bu_4NPF_6 acetonitrile solution. The onset oxidation potentials (φ_{ox}) of **P1**, **P2,** and **P3** are 1.16, 0.79, and 0.88V versus Ag/Ag$^+$, respectively. The onset reduction potentials (φ_{red}) are −0.75, −0.76, and −0.74V versus Ag/Ag$^+$, respectively. The HOMO and LUMO energy levels of the polymers were calculated according to the equations, HOMO $= -e(E_{ox} + 4.55)$ (eV), LUMO $= -e(E_{red} + 4.55)$ (eV).[44] The results of the electrochemical measurements are summarized in Table 2. The HOMO levels of polymer **P1** is around −5.71 eV. After introducing thiophene bridges between the TT and isoindigo units, **P2** and **P3** shows relatively narrow band gaps and low E_{ox} of 0.79 and 0.88 V, giving a higher HOMO level of −5.34 and −5.43 eV, respectively. Compared with **P2**, polymer **P3** depicted a lower-lying HOMO resulting in the latter polymer's slightly larger band gap. All the three polymers depicted relatively deep HOMO levels, which may lead to high V_{oc} of the BHJ PSCs. The LUMO levels of **P1**, **P2,** and **P3** are all around −3.80 eV, which indicate that the LUMO levels of these copolymers are determined by the presence of isoindigo units. The electrochemical band gaps of polymers **P1**, **P2,** and **P3** are calculated to be 1.91, 1.55, and 1.62 eV, respectively, according to the equation, $E_g^{ec} = e(E_{ox} - E_{red})$ (eV).[44] The optical band gaps of polymers **P1**, **P2,** and **P3** estimated from the absorption edges of the solid films are 1.62, 1.49, and 1.52 eV, respectively. The energy level diagrams of polymer **P1**, **P2**, **P3,** and PCBM are shown in Figure 4.

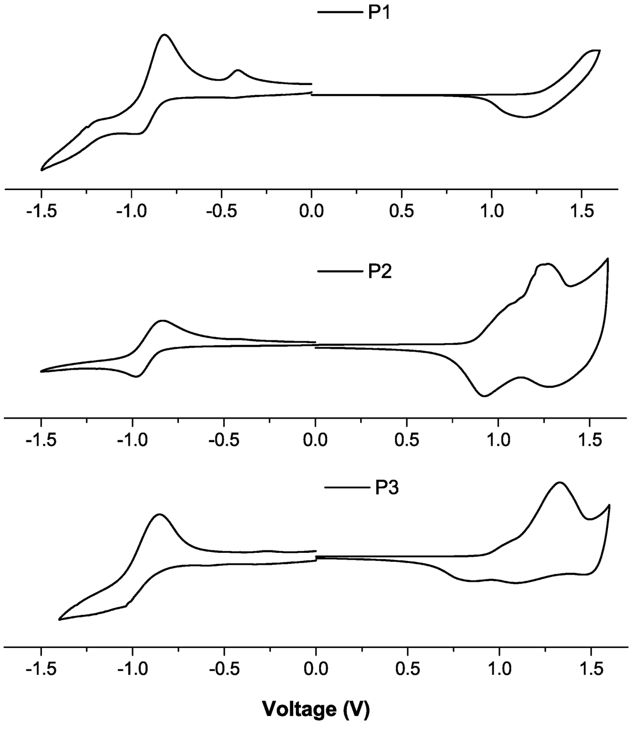

FIGURE 3 Cyclic voltammograms of polymer films on a platinum plate electrode measured in a 0.1M Bu_4NPF_6 acetonitrile solution at a scan rate of 100 mV sec^{-1}.

Photovoltaic Properties

The photovoltaic properties of polymers **P1**, **P2,** and **P3** were investigated using BHJ PSCs with configuration ITO/PEDOT:PSS (40 nm)/polymers:$PC_{71}BM$ (85 nm)/PCP-EP interlayer (4 nm)/Al (100 nm). [Fig. 5(a)]. The CB and

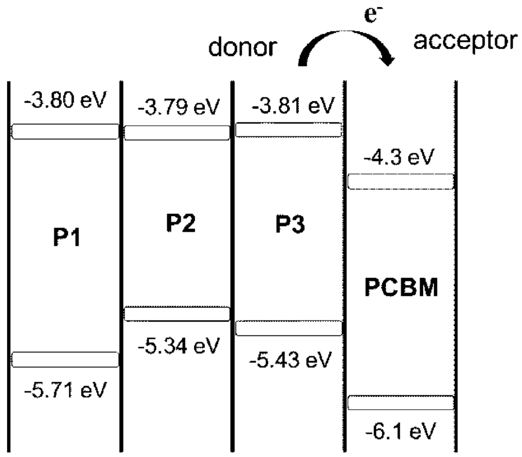

FIGURE 4 Energy level diagrams for the polymers as the donor materials in BHJ photovoltaic cells.

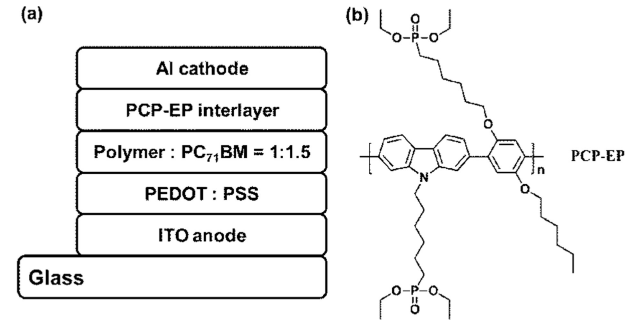

FIGURE 5 (a) The device configuration of the PSC. (b) Chemical structures of interlayer polymer PCP-EP.

TABLE 3 Photovoltaic Performances of the PSCs Based on Polymer:$PC_{71}BM$ Under the Illumination of AM1.5, 100 mW cm^{-2}

Polymers	Solvent	Ratio[a]	V_{oc} (V)	J_{sc} (mA cm^{-2})	FF (%)	PCE (%)
P1	CB	1:1.5	1.03	2.97	40.9	1.25
P2	DCB	1:1.5	0.77	4.16	58.4	1.87
P2	DCB[b]	1:1.5	0.77	9.34	65.2	4.69
P3	CB	1:1.5	0.73	7.25	59.7	3.16
P3	CB[c]	1:1.5	0.72	7.55	59.7	3.24

[a] Polymer : $PC_{71}BM$ weight ratio.
[b] 2.5% (v/v) DIO in 1,2-DCB.
[c] 2.5% (v/v) Cl-naph in CB.

1,2-dichlorobenzene (*o*-DCB) were used as the processing solvents for device fabrication. The alcohol-soluble conjugated polymer **PCP-EP** was used as the interlayer between the active layer and Al cathode. The polymer **PCP-EP** has shown good electron-injection ability in combination with high work-function Al cathode in light-emitting diodes (PLEDs).[45] These conjugated polymers with alkylphosphonates and diethanolamino side groups were used as an organic interlayer to improve interfacial contacts between the organic layer and inorganic cathode in efficient conventional and inverted solar cells.[46,47] The chemical structure of polymer **PCP-EP** is shown in Figure 5(b).

The measurements of photovoltaic performances of polymers **P1**, **P2,** and **P3** as electron donor/hole transport materials in BHJ PSCs were carried out under illumination of AM1.5G simulated solar light at 100 mW cm^{-2}. The weight ratio of polymer: $PC_{71}BM$ and thickness of the active layer was optimized. Figure 6 shows the current density–voltage (*J–V*) characteristics of PSCs. The open-circuit voltage (V_{oc}), short-circuit current (J_{sc}), fill factor (FF), and PCE of the PSCs are summarized in Table 3. For a P1:$PC_{71}BM$ weight ratio of 1:1.5 in CB, the PSC showed V_{oc}, J_{sc}, and FF of 1.03 V, 2.97 mA cm^{-2}, and 40.9%, respectively. The high V_{oc} was derived from its low HOMO level of −5.71 eV. However, the J_{sc} of **P1** was low and the PCE was 1.25%. Several solvent additives were used to optimize the morphology of the blend layer, to form favorable grain boundaries and nanostructures, thus enhancing the J_{sc} and FF for higher PCE achievement of BHJ PSCs.[32,33,48,49] Unfortunately, the PSCs based on **P1** were unresponsive to any solvent additives used. Meanwhile, in the course of device fabrication and optimization, polymer **P2** was found to afford better solubility and device performance when using *o*-DCB as the processing solvent. For a P2:$PC_{71}BM$ ratio of 1:1.5, The V_{oc}, J_{sc}, and FF of PSCs were 0.77 V, 4.16 mA cm^{-2}, and 58.4%, respectively. The calculated PCE was 1.87%. Using 1,8-diiodooctane (DIO) as the additive was effective for the PSCs based on **P2**, showing improvements of J_{sc} and FF. For a P2:$PC_{71}BM$ ratio of 1:1.5 with 2.5% (v/v) DIO in *o*-DCB, the J_{sc} and FF of PSCs exhibited an obvious increase to 9.34 mA cm^{-2} and 65.2%, respectively. The calculated PCE attained 4.69%. Compared to **P1**, the higher J_{sc} of **P2** can be attributed to its broad and red-shifted absorption spectrum and larger absorption coefficient. The lower V_{oc} of **P2** was consistent with its higher HOMO level. The good FF (0.65) of the device may indicate improved balanced charge transport of the polymer and $PC_{71}BM$. For polymer **P3**, when 1-chloronaphthalene (CI-naph) was mixed in the P3/$PC_{71}BM$ blend layer, better photovoltaic performances were obtained than those devices using the DIO additive. The CI-naph additive can reduce the solvent evaporation rate and improve the self-organization and crystallization of P3HT/PCBM blend systems.[50] For a P3:$PC_{71}BM$ ratio of 1:1.5 in CB, the V_{oc}, J_{sc}, and FF of PSCs were 0.73 V, 7.25 mA cm^{-2}, and 59.7%, respectively, corresponding to the PCE of 3.16%. After using 2.5% (v/v) CI-naph additive, the J_{sc} of PSCs depicted marginal increase to 7.55 mA cm^{-2} and the calculated PCE was up to 3.24%. As we revealed below, though polymer **P3** depicted broader and stronger absorption spectrum than **P2** due to its bithiophene-bridged D–A backbone, the morphology of P3/$PC_{71}BM$ blend layer may have a negative impact on the device performance.

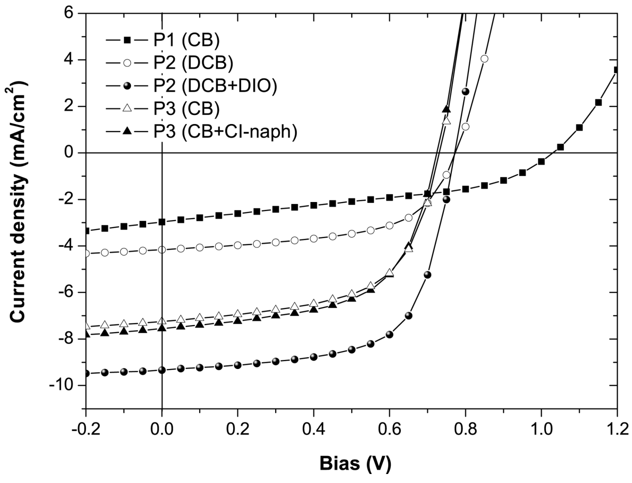

FIGURE 6 Current density–voltage (J–V) characteristics of PSCs based on polymer:$PC_{71}BM$ blends under illumination of AM1.5G, 100 mW cm^{-2}.

To verify the measurements of J_{sc}, We measured the external quantum efficiency (EQE) of the PSCs based on polymer:$PC_{71}BM$ blends under monochromatic light (Fig. 7). The

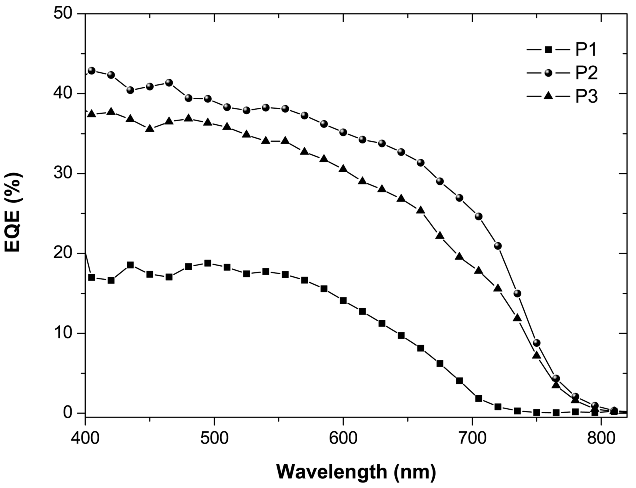

FIGURE 7 EQE curves of the PSCs with (polymer:$PC_{71}BM$ = 1:1.5) as the active layer.

maxima of the EQE are 19, 43 and 40% for **P1**, **P2,** and **P3**, respectively. The EQE curves generally correspond with UV–vis absorptions of the polymers depicting a higher value in the range from 400 to 800 nm. The enhanced quantum efficiency in the region of 400–500 nm is attributable to the high absorption intensity of $PC_{71}BM$ in the visible region, which can lead to accentuated J_{sc}.[51] The J_{sc} calculated from integration of the EQE with an AM 1.5G reference spectrum are 2.70, 8.00, and 6.68 mA cm^{-2}, respectively, which correspond to the spectral mismatch factors between 1.10 and 1.85. The mismatch factors may arise from spectral differences between the simulated solar spectrum and the AM1.5G standard spectrum.

Film Morphology

The morphology of the active layers was investigated by atomic force microscopy (AFM) (Fig. 8). The blend layers were fabricated under the respective optimized process according to the device performance. All the blend layers depicted smooth and uniform films. The root-mean-square (rms) of surface roughness was 2.1 and 2.3 nm for **P1** and **P2**, respectively. The better photovoltaic performance of **P2** was likely ascribable to the uniform interpenetrating network in the $P2/PC_{71}BM$ blend layer. Compared to **P2**, the blend layer of **P3** exhibited larger domain size and the rms roughness is up to 4.8 nm, which may be ascribed to its more rigid and inflexible backbone when using *n*-alkylthiophene as π-bridge between isoindigo and dioctylthieno[3,2-b]thiophene moieties.

Hole Mobility

Since polymer **P2** exhibited the best photovoltaic property among these four polymers, the hole mobility of the D/A blend film based on polymer **P2** was also investigated using the space charge limited current (SCLC) method. The structure of hole-only device is ITO/PEDOT:PSS/polymer $P2:PC_{71}BM$ (85 nm)/MoO_3/Al. The mobility was determined by fitting the dark current to the model of a single carrier SCLC, which is described by the equation:

$$J = \frac{9}{8}\varepsilon_0\varepsilon_r\mu_h\frac{V^2}{d^3}$$

where J is the current, μ_h is the charge mobility at zero field, ε_0 is the free-space permittivity, ε_r is the relative permittivity of the material, d is the thickness of the active layer, and V is the effective voltage. $V = V_{\mathrm{appl}} - V_{\mathrm{bi}} - V_s$, V_{appl} is the applied potential, V_{bi} is the built-in potential and V_s is the voltage drop due to the substrate series resistance. The hole-mobility can be calculated from the slope of the $J^{1/2}$–V curve (Fig. 9). The calculated mobility of the polymer **P2** is 1.9×10^{-4} cm^2 V^{-1} s^{-1}.

CONCLUSIONS

In summary, we have synthesized a novel class of thieno[3,2-b]thiophene and isoindigo-based D–A polymers, which can be used as electron donor and hole transport materials in BHJ PSCs. The polymers exhibited good thermal stability and their absorption spectral properties as well as energy levels can be tuned and optimized via thieno[3,2-b]thiophene-isoindigo repeating units and conjugated length of thiophene π-bridges. Polymer **P1** with direct D–A moieties in the backbone depicted a low lying HOMO level of −5.71 eV. In contrast, polymer **P2** containing alkylthiophene-bridged D–A backbone and corresponding alkylbithiophene-bridged polymer **P3** exhibited higher HOMO levels of around −5.4 eV

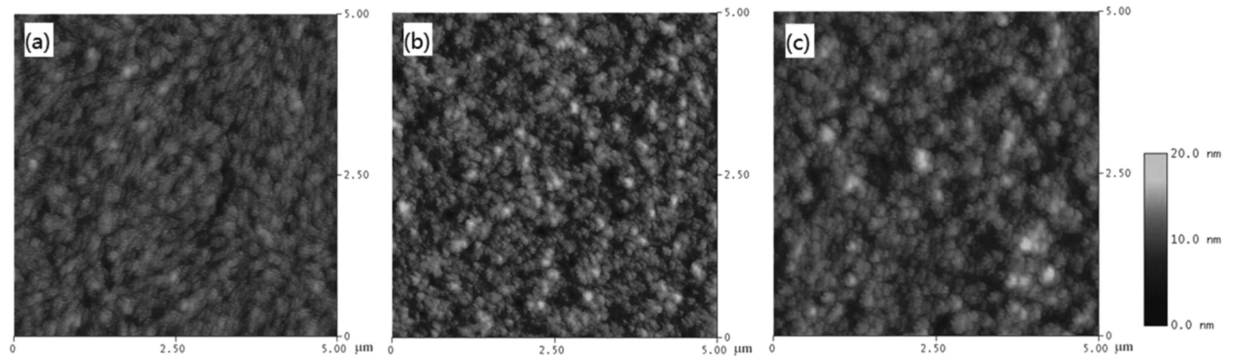

FIGURE 8 Tapping mode AFM topography images (5 × 5 μm^2) of the 1:1.5 (weight ratio) composite film of (a) $P1/PC_{71}BM$ (b) $P2/PC_{71}BM$ with 2.5% (v/v) DIO (c) $P3/PC_{71}BM$ with 2.5% (v/v) Cl-naph.

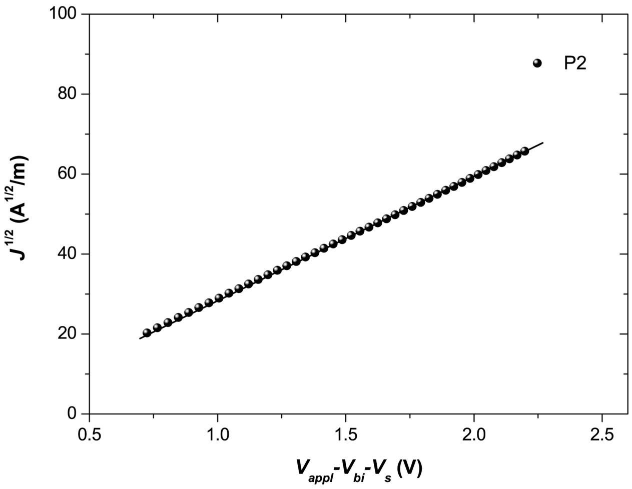

FIGURE 9 The $J^{1/2}-V$ characteristics of polymer P2 based hole-only device measured at ambient temperature.

and narrower band gaps. In comparison to **P1**, polymer **P2**, which has an alkylthiophene π-bridge between D–A units, can depict broad, red-shifted absorptions over the 400–800 nm region. In addition, although polymer **P3** can extend the coplanarity of polymer main chain and improve absorption spectrum somewhat by using the alkylbithiophene π-bridge, polymer **P2** nonetheless depicted better solubility, larger absorption coefficient, more uniform and interpenetrating polymer/$PC_{71}BM$ components in the active layer, which afforded accentuated device performances. A reasonably good PCE of about 4.7% has been achieved using polymer **P2** as electron donor and hole transport polymers in conventional BHJ PSCs. The results attest that the application of the D–π–A structure with selected donor moiety and the π-bridges can be seen as a feasible method in synthesis of isoindigo-based copolymers for efficient BHJ PSCs. We believe that through further structural optimization on the isoindigo-based D–π–A polymers, higher performing BHJ PSCs can be fabricated.

ACKNOWLEDGMENTS

The authors acknowledge financial support from the A*STAR SERC grant (Grant no: 102 170 0135) and National Natural Science Foundation of China (Grant no: 51173048).

REFERENCES AND NOTES

1 Tang, C. W. *Appl. Phys. Lett.* **1986,** *48*, 183–185.

2 Kim, J. Y.; Lee, K.; Coates, N. E.; Moses, D.; Nguyen, T.-Q.; Dante, M.; Heeger, A. J. *Science* **2007,** *317*, 222–225.

3 Yu, G.; Gao, J.; Hummelen, J. C.; Wudl, F.; Heeger, A. J. *Science* **1995,** *270*, 1789–1791.

4 Gunes, S.; Neugebauer, H. S.; Sariciftci, N. S. *Chem. Rev.* **2007,** *107*, 1324–1338.

5 Thompson, B. C.; Frechet, J. M. J. *Angew. Chem. Int. Ed.* **2008,** *47*, 58–77.

6 Brabec, C. J.; Sariciftci, N. S.; Hummelen, J. C. *Adv. Funct. Mater.* **2001,** *11*, 15–26.

7 Li, Y. F.; Zou, Y. P. *Adv. Mater.* **2008,** *20*, 2952–2958.

8 Cheng, Y. J.; Yang, S. H.; Hsu, C. S. *Chem. Rev.* **2009,** *109*, 5868–5923.

9 Chen, J. W.; Cao, Y. *Acc. Chem. Res.* **2009,** *42*, 1709–1718.

10 Liang, Y. Y.; Yu, L. P. *Acc. Chem. Res.* **2010,** *43*, 1227–1236.

11 Zhou, H. X.; Yang, L. Q.; You, W. *Macromolecules* **2012,** *45*, 607–632.

12 Bian, L. Y.; Zhu, E. W.; Tang, J.; Tang, W. H.; Zhang, F. J. *Prog. Polym. Sci.* **2012,** *37*, 1292–1331.

13 Hoppe, H.; Sariciftci, N. S. *J. Mater. Chem.* **2006,** *16*, 45–61.

14 He, Z. C.; Zhang, C.; Xu, X. F.; Zhang, L. J.; Huang, L.; Chen, J. W.; Wu, H. B.; Cao, Y. *Adv. Mater.* **2011,** *23*, 3086–3089.

15 Seo, J. H.; Gutacker, A.; Sun, Y.; Wu, H.; Huang, F.; Cao, Y.; Scherf, U.; Heeger, A. J.; Bazan, G. C. *J. Am. Chem. Soc.* **2011,** *133*, 8416–8419.

16 He, Z. C.; Zhong, C. M.; Huang, X.; Wong, W. Y.; Wu, H. B.; Chen, L. W.; Su, S. J.; Cao, Y. *Adv. Mater.* **2011,** *23*, 4636–4637.

17 Chen, H. Y.; Hou, J. H.; Zhang, S. Q.; Liang, Y. Y.; Yang, G. W.; Yang, Y.; Yu, L. P.; Wu, Y.; Li, G. *Nat. Photonics* **2009,** *3*, 649–653.

18 Wang, E. G.; Hou, L. T.; Wang, Z. Q.; Hellström, S.; Zhang, F. L.; Inganäs, O.; Andersson, M. R. *Adv. Mater.* **2010,** *22*, 5240–5244.

19 Zhang, Y.; Zou, J. Y.; Yip, H. L.; Chen, K. S.; Zeigler, D. F.; Sun, Y.; Jen, A. K. Y. *Chem. Mater.* **2011,** *23*, 2289–2291.

20 Zhou, H. X.; Yang, L. Q.; Stuart, A. C.; Price, S. C.; Liu, S. B.; You, W. *Angew. Chem. Int. Ed.* **2011,** *123*, 3051–3054.

21 Price, S. C.; Stuart, A. C.; Yang, L. Q.; Zhou, H. X.; You, W. *J. Am. Chem. Soc.* **2011,** *133*, 4625–4631.

22 Wang, M.; Hu, X. W.; Liu, P.; Li, W.; Gong, X.; Huang, F.; Cao, Y. *J. Am. Chem. Soc.* **2011,** *133*, 9638–9641.

23 Amb, C. M.; Chen, S.; Graham, K. R.; Subbiah, J.; Small, C. E.; So, F.; Reynolds, J. R. *J. Am. Chem. Soc.* **2011,** *133*, 10062–10065.

24 Ong, K. H.; Lim, S. L.; Tan, H. S.; Wong, H. K.; Li, J.; Ma, Z.; Moh, L. C. H.; Lim, S. H.; de Mello, J. C.; Chen, Z. K. *Adv. Mater.* **2011,** *23*, 1409–1413.

25 Chang, C. Y.; Cheng, Y. J.; Hung, S. H.; Wu, J. S.; Kao, W. S.; Lee, C. H.; Hsu, C. S. *Adv. Mater.* **2012,** *24*, 549–553.

26 Du, C.; Li, C. H.; Li, W. W.; Chen, X.; Bo, Z. S.; Veit, C.; Ma, Z. F.; Wuerfel, U.; Zhu, H. F.; Hu, W. P.; Zhang, F. L. *Macromolecules* **2011,** *44*, 7617–7624.

27 Small, C. E.; Chen, S.; Subbiah, J.; Amb, C. M.; Tsang, S. W.; Lai, T. H.; Reynolds, J. R.; So, F. *Nat. Photonics* **2012,** *6*, 115–120.

28 Mei, J. G.; Graham, K. R.; Stalder, R.; Reynolds, J. R. *Org. Lett.* **2010,** *12*, 660–663.

29 Stalder, R.; Mei, J. G.; Reynolds, J. R. *Macromolecules* **2010,** *43*, 8348–8352.

30 Stalder, R.; Mei, J. G.; Subbiah, J.; Grand, C.; Estrada, L. A.; So, F.; Reynolds, J. R. *Macromolecules* **2011,** *44*, 6303–6310.

31 Zhang, G. B.; Fu, Y. Y.; Xie, Z. Y.; Zhang, Q. *Macromolecules* **2011,** *44*, 1414–1420.

32 Wang, E. G.; Ma, Z. F.; Zhang, Z.; Henriksson, P.; Inganäs, O.; Zhang, F. L.; Andersson, M. R. *Chem. Commun.* **2011,** *47*, 4908–4910.

33 Ma, Z. F.; Wang, E. G.; Jarvid, M. E.; Henriksson, P.; Inganäs, O.; Zhang, F. L.; Andersson, M. R. *J. Mater. Chem.* **2012,** *22*, 2306–2314.

34 Wang, E. G.; Ma, Z. F.; Zhang, Z.; Vandewal, K.; Henriksson, P.; Inganäs, O.; Zhang, F. L.; Andersson, M. R. *J. Am. Chem. Soc.* **2011,** *133*, 14244–14247.

35 Lei, T.; Cao, Y.; Fan, Y. L.; Liu, C. J.; Yuan, S. C.; Pei, J. *J. Am. Chem. Soc.* **2011,** *133*, 6099–6101.

36 Ong, B. S.; Wu, Y. L.; Li, Y. N.; Liu, P.; Pan, H. L. *Chem. Eur. J.* **2008,** *14*, 4766–4778.

37 Zhang, X. N.; Köhler, M.; Matzger, A. J. *Macromolecules* **2004,** *37*, 6306–6315.

38 Mcculloch, I.; Heeney, M.; Bailey, C.; Genevicius, K.; Macdonald, I.; Shkunov, M.; Sparrowe, D.; Tierney, S.; Wagner, R.; Zhang, W. M.; Chabinyc, M. L.; Kline, R. J.; Mcgehee, M. D.; Toney, M. F. *Nat. Mater.* **2006,** *5*, 328–333.

39 Li, Y. N.; Singh, S. P.; Sonar, P. *Adv. Mater.* **2010,** *22*, 4862–4866.

40 Bronstein, H.; Chen, Z. Y.; Ashraf, R. S.; Zhang, W. M.; Du, J. P.; Durrant, J. R.; Tuladhar, P. S.; Song, K.; Watkins, S. E.; Geerts, Y.; Wienk, M. M.; Janssen, R. A. J.; Anthopoulos, T.; Sirringhaus, H.; Heeney, M.; McCulloch, I. *J. Am. Chem. Soc.* **2011,** *133*, 3272–3275.

41 Li, Y. L.; Wu, Y. L.; Liu, P.; Birau, M.; Pan, H. L.; Ong, B. S. *Adv. Mater.* **2006,** *18*, 3029–3032.

42 Rieger, R.; Beckmann, D.; Pisula, W.; Kastler, M.; Müllen, K. *Macromolecules* **2010,** *43*, 6264–6267.

43 Wu, H. B.; Huang, F.; Mo, Y. Q.; Yang, W.; Wang, D. L; Peng, J.; Cao, Y. *Adv. Mater.* **2004,** *16*, 1826–1830.

44 Scharber, M. C.; Mühlbacher, D.; Koppe, M.; Denk, P.; Waldauf, C.; Heeger, A. J.; Brabec, C. J. *Adv. Mater.* **2006,** *18*, 789–794.

45 Xu, X. F.; Han, B.; Chen, J. W.; Peng, J. B.; Wu, H. B.; Cao, Y. *Macromolecules* **2011,** *44*, 4204–4212.

46 Zhu, Y. X.; Xu, X. F.; Zhang, L. J.; Chen, J. W.; Cao, Y. *Sol. Energy Mater. Sol. Cells* **2012,** *97*, 83–88.

47 Xu, X. F.; Zhu, Y. X.; Zhang, L. J.; Sun, J. M.; Huang, J.; Chen, J. W.; Cao, Y. J. *J. Mater. Chem.* **2012,** *22*, 4329–4336.

48 Liang, Y. Y.; Feng, D. Q.; Wu, Y.; Tsai, S. T.; Li, G.; Ray, C.; Yu, L. P. *J. Am. Chem. Soc.* **2009,** *131*, 7792–7799.

49 Szarko, J. M.; Guo, J. C.; Liang, Y. Y.; Lee, B.; Rolczynski, B. S.; Strzalka, J.; Xu, T.; Loser, S.; Marks, T. J.; Yu, L. P.; Chen, L. X. *Adv. Mater.* **2010,** *22*, 5468–5472.

50 Chen, F. C.; Tseng, H. C.; Ko, C. J. *Appl. Phys. Lett.* **2008,** *92*, 103316.

51 Wienk, M. M.; Kroon, J. M.; Verhees, W. J. H.; Knol, J.; Hummelen, J. C.; van Hal, P. A.; Janssen, R. A. J. *Angew. Chem. Int. Ed.* **2003,** *42*, 3371–3375.